Understanding the electrolytic generation of sulfate and chlorine oxidative species with different boron-doped diamond anodes

Géssica O. S. Santos[a,b,c], Katlin I. B. Eguiluz[a,b], Giancarlo R. Salazar-Banda[a,b], Cristina Saez[c], Manuel A. Rodrigo[c,*]

[a] *Electrochemistry and Nanotechnology Laboratory, Research and Technology Institute, Aracaju, SE, Brazil*

[b] *Processes Engineering Post-graduation - PEP, Universidade Tiradentes, 49037-580 Aracaju, SE, Brazil*

[c] *Department of Chemical Engineering, Universidad de Castilla-La Mancha, Campus Universitario s/n, 13071 Ciudad Real, Spain*

Abstract

The electrochemical generation of several oxidative species was studied at the surfaces of five commercial boron-doped diamond anodes with different doping levels (100–8000 ppm). These insights can open the possibility of tailoring anodes for a more efficient application in environmental remediation processes. All materials evaluated were characterized by linear sweep voltammetry, cyclic voltammetry, electrochemical impedance spectroscopy, contact angle, and scanning electron microscopy, as well as by bulk electrolysis. As a result, it was confirmed that the boron doping level influences the physical and electrochemical properties of the electrodes, indicating distinct behavior of the electrodes on the production of chlorine and sulfate oxidative species. The higher the boron doping, the lower is the crystallite size, and the higher is the conductivity, the hydrophilic behavior, and the electron-transfer activity.

Voltammetric characterization demonstrates that low boron doping favors the formation of hydroxyl radicals, while high doping levels favor the direct electrochemical oxidation of sulfate or chloride. Moreover, when operating at high overpotentials in bulk electrolysis (typical conditions in environmental applications), the formation of chlorine and sulfate oxidative species is favored at low boron doping levels. This behavior is attributed to the very efficient mediated formation of these oxidants from the hydroxyl radicals, whose production is promoted with these electrodes at those conditions. It means that only operating at much softer conditions, the unique direct generation of hydroxyl oxidant occurs, opening a way for the potential prevention of perchlorate formation during disinfection by using highly boron-doped diamond anodes.

Keywords: Diamond; oxidants; chlorine; persulfate; mechanisms; perchlorate.

Highlights

- Higher boron doping attains higher hydrophilicity and conductivity of the anode
- Higher boron doping levels promote electron transfer activity
- Thickness of BDD layer and Si-resistivity influence the electron-transfer ability
- Low boron doping favors the formation of hydroxyl radicals
- High doping levels favor the direct oxidation of sulfate and chloride

* Author to whom all correspondence should be addressed (manuel.rodrigo@uclm.es)

1. Introduction

For many years, boron-doped diamond (BDD) films have been a subject of considerable interest. It has been proposed as an excellent electrode material for various applications, due to its outstanding properties, such as a wide potential window [1], high pollutant removal efficiency in wastewater treatment processes [2-4], high efficiencies in the production of oxidants [5] and outstanding features for electroanalysis [6, 7]. It has been proved, that the properties of BDD anodes are affected by many factors, such as concentration and type of the dopant; morphological properties, primary crystallographic orientation, surface termination (H, O, F, etc.), grain boundaries, and the presence of non-diamond carbon phases [8-12].

Electrochemical oxidation is considered as one of the most promising advanced oxidation technologies, because of the ability of boron-doped diamond (BDD) electrodes to generate hydroxyl radicals ($^{\bullet}OH$), which makes them been selected for the degradation of persistent organic contaminants [13, 14]. The high activity of BDD anode toward organics oxidation has been explained by the presence of weakly adsorbed $^{\bullet}OH$ formed by water electrolysis at the anode surface (Eq. 1) [15], in the so-called "non-active" behavior of this electrodes.

$$BDD + H_2O \rightarrow BDD\,(^{\bullet}OH) + H^+ + e^- \quad (1)$$

The effectiveness of the electrochemical oxidation of organics in water depends on many factors, including the presence of species in solution able to act as mediators. Thus, it has been studied the formation of different oxidants depending on the electrolyte composition [16]. Accordingly, chloride can be oxidized not only to chlorine but also to other chlorinated species such as chlorate and perchlorate [17]. Sulfate can be oxidized to peroxosulfate, being a typical representative of the family of peroxocompounds, which also include other species such as the peroxocarbonate and peroxophosphate (which are produced from carbonates and phosphates, respectively) [5, 18]. Besides, oxidation of water, oxygen or decomposition of oxidants

produced anodically can explain the observed formation of other oxidants such as ozone or hydrogen peroxide (whose formation can also be explained in terms of the cathodic reduction of oxygen) [19].

In considering electrochemical processes, the two most important anions in water from the viewpoint of the electrochemical treatment are chloride and sulfate, because of the relevance of the oxidants produced. Besides, interactions between the oxidants produced and irradiation of UV, or application of ultrasounds, can promote the formation of radical oxidants from the species previously commented. As a result, an essential cocktail of mixed oxidants is produced during the electrolysis of almost any type of wastewater [15].

Properties of diamond coatings can influence the mechanisms of formation of oxidants, as well as influence the direct electrochemical oxidation processes. The formation of oxidants from oxidant precursor on the surface of the diamond anode is the primary step in the direct electrochemical oxidation. Because of that, it is vital to know, for tailoring diamond for different applications, the effect of the most critical parameter, that is, the boron doping level [20, 21], which is known to affect not only to the electrode conductivity but also to its performance.

Here, we present evidence about the influence of boron doping on the production of chlorine and sulfate oxidative species during electrolysis of wastewater. The results obtained will help to develop a correlation between physical and electrochemical properties of this important anode material, as well as to understand the oxidation mechanisms happening onto these anodes, in search of new approaches for tailoring BDD for different applications.

2. Methodology

2.1 Chemicals

To determine oxidants KI, $Na_2S_2O_3$, NaOH, As_2O_3, and starch solution (1 %) were purchased from Sigma-Aldrich. The electrolyte solution was prepared by 3.0 g L^{-1} Na_2SO_4 (Panreac) or

3.7 g L^{-1} of NaCl (Panreac) and H_2SO_4 0.5 mol L^{-1} (Sigma Aldrich). All solutions were prepared using high-purity water (Millipore Milli-Q system, resistivity >18 MΩ cm). All reactants were used as received

2.2 Electrodes

BDD films were provided by Adamant Technologies (Neuchatel, Switzerland) and synthesized by the hot-filament chemical vapor deposition technique (HF CVD) on single crystal p-type Si (1 0 0) wafers (Siltronix). The main characteristics of the BDD anodes selected for this study are summarized in Table 1.

Table 1. Main characteristics of different BDD anodes used in this work (provided from Adamant Technologies).

Anode	Boron content /ppm	Ratio sp^3/sp^2	Thickness BDD layer / µm	Si-resistivity / Ω	Roughness, Si-Surfinra / µm
BDD8000	8000	80	1.05	10	< 0.1
BDD2500	2500	43	1.13	10	< 0.1
BDD1300	1300	77	2.27	10	0.3 – 0.5
BDD200	200	75	1.14	100	0.3 – 0.5
BDD100	100	89	1.03	10	0.3 – 0.5

2.3 Physical characterization

The morphology of the surfaces of the BDD films was visualized through field-emission scanning electron microscope (FE-SEM; Zeiss GeminiSEM 500). Sessile drop contact angle and surface tension measurements were carried out on an Attension Theta Lite Optical Tensiometer. Tests were always performed immediately after the drop falls on the surface. Thus, the drop profile is analyzed by the video camera and processed by the OneAttension

Software in order to obtain Contact angle, CA (Θ), and surface tension, ST, (mN m^{-1}) between the diamond layer and liquid drop high-purity water at room temperature and atmospheric pressure.

2.4 Electrochemical measurements

The electrochemical measurements were performed in a conventional three-electrode cell connected to a computer-controlled Autolab potentiostat/galvanostat model PGCTAT 302N. The cell used Ag/AgCl (3 M KCl) as a reference electrode and platinum (Pt) as a counter electrode. The working electrodes used were BDD anodes of 4 cm^2 of geometric area. CV measurements were performed at the potential limits of −0.7–+1.1 V with a scan rate of 100 mV s^{-1} in a solution of $[Fe(CN)_6]^{3-/4-}$ 0.01 mol L^{-1} in 0.1 mol L^{-1} Na_2SO_4. Linear sweep voltammetry experiments were performed in the potential interval of 0.0–2.7 V. The electrochemical impedance spectroscopy measurements were obtained covering the frequency range of 0.1 Hz–10 kHz using an AC sine signal amplitude of 5 mV.

2.5 Analytical procedures

Inorganic anions (Cl^-, ClO_3^- and ClO_4^-) were determined by ion chromatography 930 Compact IC Flex (Metrohm) (column: MetrosepASupp 4; flow rate: 0.8 mL min^{-1}). As for hypochlorite, due to interference with the chloride peak in the chromatogram, titration with As_2O_3 in NaOH 2M was employed. Oxidants were determined by iodometric titration.

3. Results and discussion

3.1 Physical characterization – SEM and Contact Angle

The morphological characterization of diamond films is essential to understand differences among distinct BDDs films studied. Thus, the surface of the BDD films (100 ppm– 8000 ppm) investigated by SEM are presented in **Figure 1(a−e)**. SEM data shows that the boron content

influences the film morphology, although all BDD films are polycrystalline, presenting randomly-oriented grain sizes. The BDD8000 film presents a more uniform grain distribution with the smallest crystals sizes on its surface. The BDD2500 and BDD1300, are characterized by an increase in grain size in some regions, meaning a less homogeneous distribution on the surface. On the contrary, the BDD100 and BDD200 films show larger crystal sizes well-distributed onto its surface. The decrease in the grain size with increasing boron content has been reported for other BDDs films [8, 12]. Matsushima *et al*. [12] pointed out that the average grain size remained between 6.0 and 4.8 μm for films with 2,000 and 20,000 ppm, respectively, indicating a decrease in the grain size with the increase in the boron concentration during the grown of the films. Several authors demonstrated that, due to secondary nucleation promoted by boron incorporation, the average crystallites size decreases [22]. A consequence of the increasing doping level is the improved conductivity, explained because the smaller crystallites give higher surface roughness and in turn, more electroactive sites for reactions to occur.

Moreover, surface termination plays a vital role in the applicability of BDD electrodes. Contact angle (CA) measurements of BDD films employing a drop of high-purity water placed on its surfaces (**Figure 1 (f−j))** provide information about the surface termination associated with the doping level.

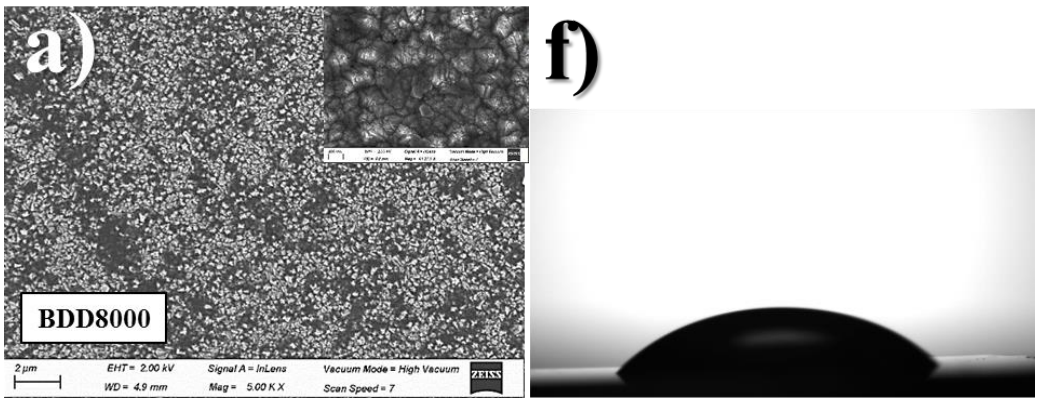

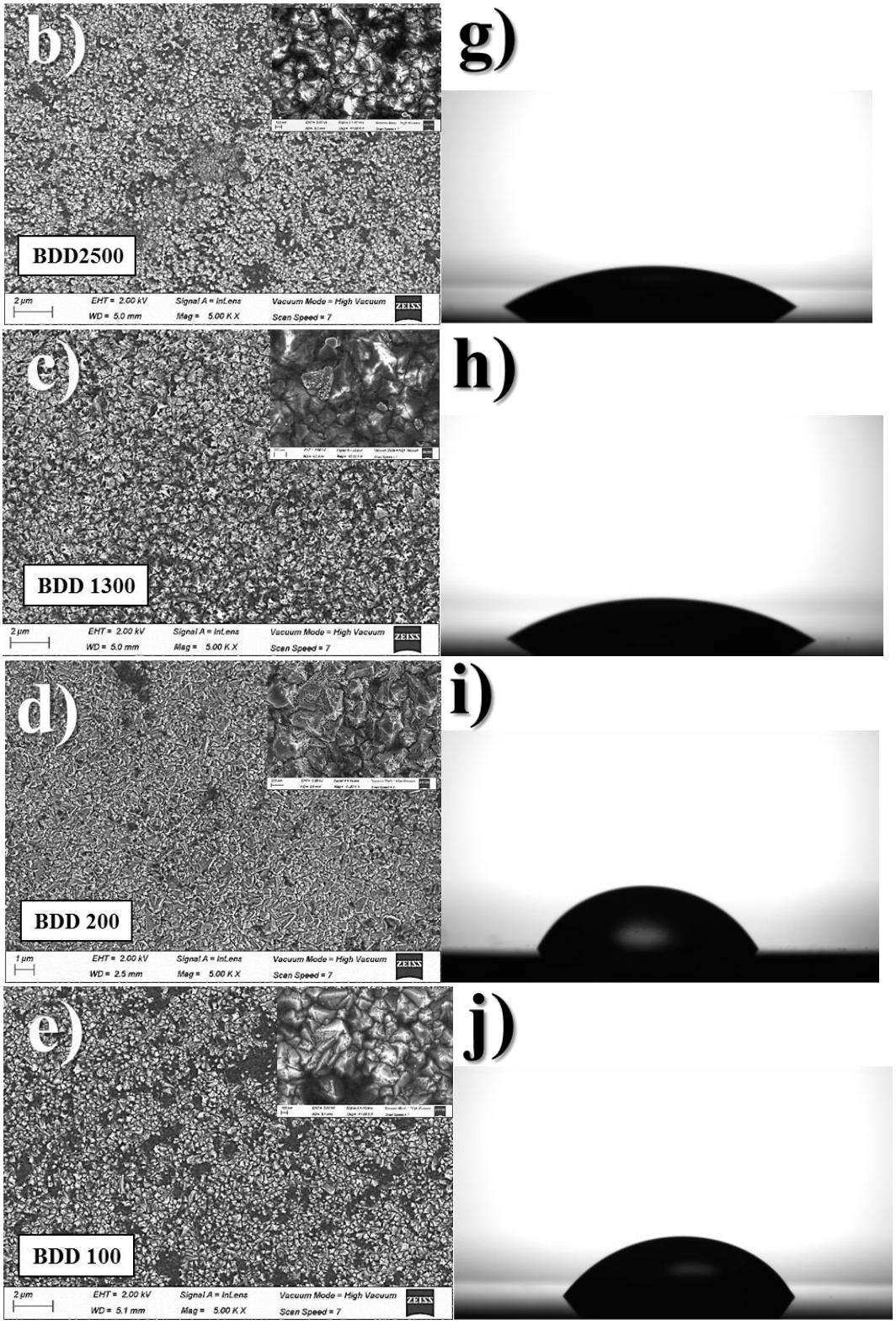

Figure 1. Scanning electron micrographs (a – e) and contact angle (f – j) of the surface of BDD films with boron content of BDD8000 (a + f), BDD2500 (b + g), BDD1300 (c + h), BDD200 (d + i) and BDD100 (e + j). SEM images with magnification of 5000× (insets images with magnification of 41,000×).

Contact angle and surface tension values are summarized in **Table 2**. In this table, it is also included the standard deviation of all measurements (three different regions of the film surface were assessed). All surface tension values were very close to each other, being the lowest value of 50.22 ± 17.18 mN m^{-1} (BDD2500) and the highest 59.76 ± 10.71 mN m^{-1} (BDD200). The lower values obtained by the highly doped diamond surfaces (as a general trend) informs about a more hydrophilic behavior and, thus, of the presence of terminations which can interact easily with water. Thus, the surface of doped films has stronger interactions with the water molecules, probably due to the formation of oxygen-containing functional groups that serve as an active center of water wetting [12, 23, 24]. It has been reported that the higher contact angle, the higher water resistance of coatings, which was associated with the minimization of attack of corrosive ions onto the film surface through fissures [25]. It is worthwhile to point out the peculiar behavior of the BDD1300 diamond. The lowest contact angle of this anode can be explained by two distinct characteristics: the larger thickness of this diamond coating and its higher Si-substrate roughness (see Table 1). Hence, the growth of a thicker layer in this substrate favors deposition of films with higher surface area which can be another critical factor influencing wettability. Thus, the higher the surface area, more active centers of water wetting.

Table 2. Average contact angle and surface tension values measured with high-purity water drop at the liquid-solid interface of different BBD surfaces

Anode	**Surface tension ± SD / mN m^{-1}**	**Contact Angle ± SD / degrees**
BDD*8000*	54.50 ± 7.66	44.72 ± 3.90
BDD*2500*	50.22 ± 17.18	44.74 ± 5.71
BDD*1300*	52.92 ± 10.93	34.22 ± 2.24
BDD*200*	59.76 ± 10.71	57.27 ± 5.39

BDD*100*	58.53 ± 15.34	50.82 ± 6.12

SD – standard deviation.

3.2 Electrochemical characterization of BDDs

A study of CVs of $[Fe(CN)_6]^{3-/4-}$ as inner-sphere redox marker was carried out to evaluate the electrochemical behavior of BBD films (Figure 2), in anodic and cathodic potential regions. $[Fe(CN)_6]^{3-/4-}$ as redox couple is well known for producing an inner-sphere redox system with carbon-based electrodes, in which the electron transfer occurs through interaction with the reactive sites on the electrode surface. Reactive sites are generally proposed to be impurities, surface defects, and surface functional groups [8].

Higher reversibility is observed for the anodes with higher doping levels (BDD1300–BDD8000), indicating better electrocatalytic properties. The higher peak-to-peak potential separation of the BDD200 is a result of the higher resistivity of the silicon substrate, which seems to be a significant parameter from the electrochemical point of view, although it is not the real interface between the electrode and the electrolyte. Thus, in comparing the performance of the BDD100 and BDD200 coatings, the relevance of this parameter can be highlighted. Its relevance in oxidative processes was pointed out in a previous report in which it was demonstrated that thinner layers favor the formation of the oxidant peroxophosphate [26].

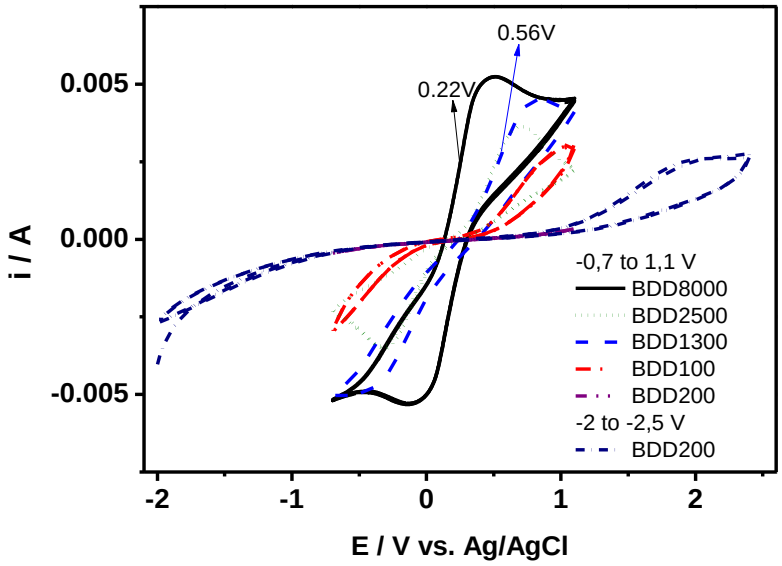

Figure 2. Cyclic voltammograms of $[Fe(CN)_6]^{3-/4-}$ (0.01 mol L^{-1} in 0.1 mol L^{-1} Na_2SO_4) measured at BDD electrode with different boron content: (a) 8000 ppm, (b) 2500 ppm, (c) 1300 ppm, (d) 200 ppm, (e) 100 ppm. Scan rate v = 100 mV s^{-1}.

Electrochemical impedance spectroscopy was used to investigate the electron transfer capacity of the BBD anodes. The well-developed semi-circles observed in the presence of $[Fe(CN)_6]^{3-/4-}$ **(Figure 3)** is in accordance with other studies found in the literature [27].

Figure 3 (part b and part c) shows the equivalent circuit used to fit the Nyquist plots (Fig. 3a). In the case of BDD2500, BDD1300, BDD200, and BDD100, the spectra are well-described by the equivalent circuit represented by $R_s(R_fC_f)(R_{ct}C_{dl})$ (Fig. 3b). In this circuit, the ohmic resistance R_s of the electrolyte solution, electrodes, and contacts are in series with the parallel combination of pseudo-capacitance and resistance of interface Si substrate/BDD film, followed by pseudo-capacitance associated with electrical double-layer (dl) and charge transfer resistance associated with BDD film/electrolyte interface. The use of pseudo-capacitances (CPE) instead of pure capacitors (C) for diamond electrodes is usually justified by the complicated surface morphology, which is responsible for the heterogeneous nature of the BDD film surface: poly-crystalline with grain boundaries, edges, and facets [28, 29]. Thus, the use

of a CPE to replace the double-layer capacitance (C_{dl}) can be written, as shown in Eq. 2, where Y_0 is CPE constant, the exponent n is a parameter varying from 0 to 1.0 applied to situations where a single capacitor cannot describe interfacial capacitance, e.g., when a dispersive character of system occurs (when n =1, then the CPE corresponds to the capacitance C), w is the angular frequency ($2\pi f$), f is the frequency and j is the imaginary number ($j = \sqrt{-1}$).

$$Z_{CPE} = \frac{1}{Y_0(jw)^n} \quad (2)$$

In the case of BDD8000, the pseudo-capacitance and resistance of the interface Si substrate/BDD film are not undoubtedly seen. It occurs when the film has very high conductive properties, which impossibilities R_fC_f to be visualized. Thus, for this anode, the impedance spectrum is well-described by the equivalent circuit represented by $R_s(R_{ct}C_{dl})$ (Fig. 3c).

All impedance data fitted well with the proposed equivalent circuits displaying fitting quality factor $\chi^2 < 5\times10^{-4}$, which is an indication of the quality of the fitting.

Moreover, **Figure 3** indicates that the boron content influences the charge transfer rate at the BDD films. The highly doped BDD films (8000–1300 ppm) exhibit semi-metallic conductivity due to the impurity bands of low energy that allow electron conduction, which is reflected in low charge transfer resistances. As expected, the BDD8000, due to its very high conductivity, has the lowest charge transfer resistance value of 26.6 Ω. However, BDD2500 and BDD1300 do not follow that trend, which can be explained by the effect of other parameters influencing the electron transfer. Thus, the thickness of the diamond layer may help to explain the lower electron transfer resistance of the BDD1300 (127.3 Ω) than the BDD2500 (247.7 Ω). In this case, the higher thickness (2.27 μm) of the BDD1300 seems to influence positively on the reaction rate, as compared to the BDD2500, with a lower thickness (1.13). This result is in agreement with results previously found in the oxidation of enrofloxacin, where surprisingly, the direct electrochemical activity is promoted in the electrode with the thicker diamond layer [30]. On the other hand, lower doping levels (100 and 200 ppm) result in semi-conductive

properties (low conductivity). The higher charge transfer resistance of the BDD200 than the BDD100 can be explained by the higher substrate resistivity of this electrode, as it was previously pointed out in the CV behavior.

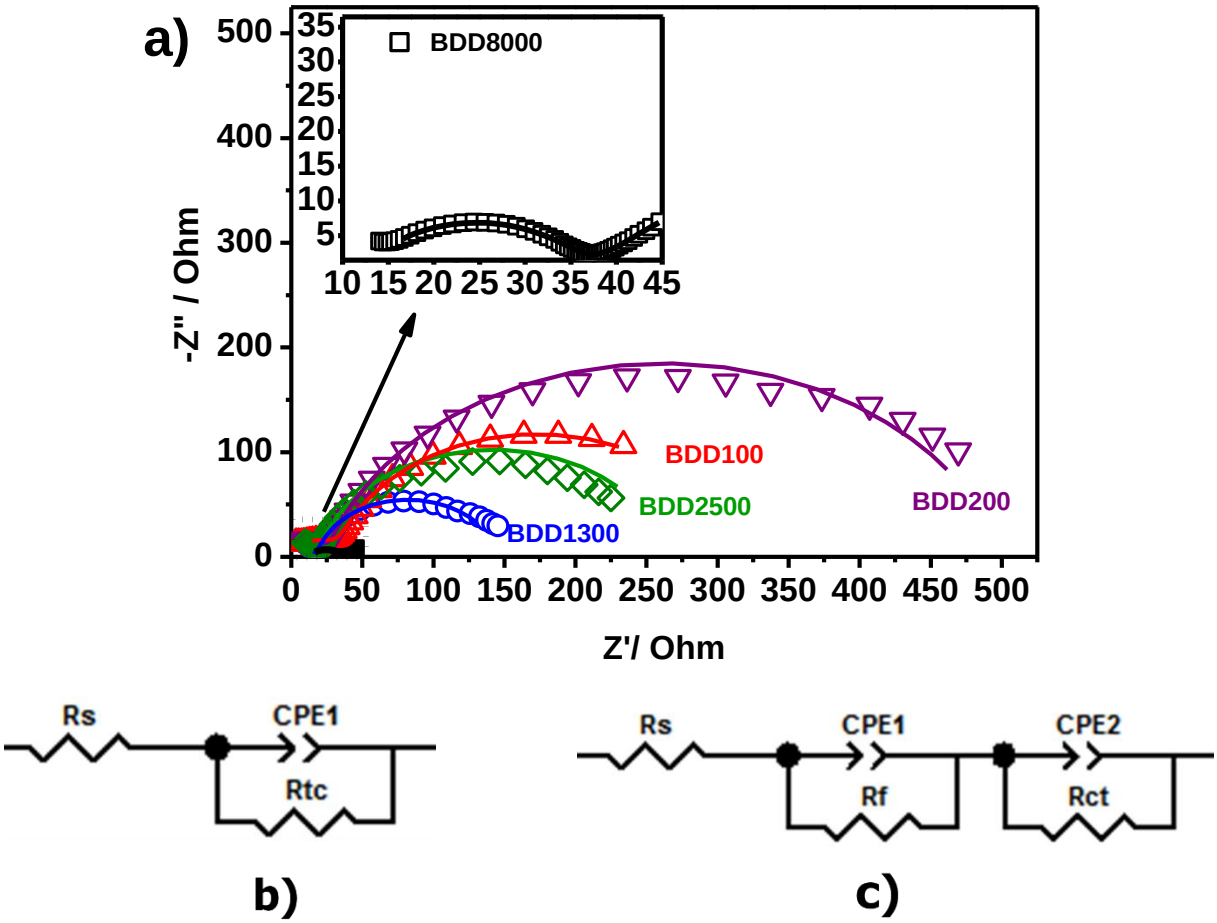

Figure 3. Nyquist plots (a) of the BDD anodes (100 ppm – 8000 ppm) at the potential determined from CV analysis vs. Ag/AgCl reference electrode in $[Fe(CN)_6]^{3-/4-}$ 0.010 mol L^{-1} in 0.1 mol L^{-1} Na_2SO_4. Frequency range: 0.1 Hz ≤ f ≤ 100 kHz. Equivalent circuits used to fit the electrochemical impedance spectra for BDD8000 (b) and BDD2500 to BDD100 (c) (R_s is the ohmic serial resistance, CPE is the constant phase element, R_f is the film resistance and, R_{ct} is the associated charge transfer resistance).

Table 3. EIS fitting data obtained by fitting experimental spectra for the electron-transfer ability for the redox couple $Fe(CN)_6]^{3-/4-}$ 0.010 mol L^{-1} in 0.1 mol L^{-1} Na_2SO_4.

Anode	R_s / Ω	Q_f / *F*	R_f / Ω	n_1	Q_{dl} / *F*	R_{ct} / Ω	n_2	χ^2
BDD8000	11.46	–	–	–	3.4×10^{-4}	26.6	0.61	7.4×10^{-5}

BDD2500	2.1×10^{-4}	3.46×10^{-7}	18.32	0.89	2.9×10^{-5}	247.4	0.88	3.7×10^{-4}
BDD1300	1.19×10^{-7}	5.9×10^{-6}	18.52	0.66	1.66×10^{-5}	127.3	0.90	5.7×10^{-4}
BDD200	8×10^{-7}	7.3×10^{-7}	26.14	0.86	7.4×10^{-6}	423.8	0.86	7.8×10^{-5}
BDD100	9.3×10^{-5}	1.67×10^{-6}	33.16	0.83	1.05×10^{-5}	279.4	0.88	5.0×10^{-5}

a. Reactive sulfate species formation

The quantity of oxidants produced during electrooxidation in Na_2SO_4 media is supposed to be influenced by the BDD anode properties [31]. Thus, it is vital to study the oxygen evolution overpotentials by using linear sweep voltammetry (LSV) in the aqueous Na_2SO_4 media (**Figure 4**).

The oxygen evolution overpotential decreases with the increasing boron doping level. Tafel slopes (Eq. 3) are an essential parameter to be considered because they stand for individual processes [32].

$$\eta = a + b \log j \quad (3)$$

Tafel plots show two processes (fitting slopes are in Table 4). The first slope corresponds to the oxidation of sulfate to sulfate radical and increases with the increase of the doping of the coating. The second is the OER, and the slope follows the opposite trend. It means that high boron doping favors the formation of sulfate radicals, while low doping favors the formation of hydroxyl radicals. As the behaviors of both radicals are not similar, this can help to explain the important differences observed with the boron doping level of the diamond coating. Recombination of radicals leads to the formation of stable oxidants such as hydrogen peroxide, monoperoxosulfuric acid, or peroxodisulfuric acid (Eq. 4−6). Besides, further interactions of these oxidants lead to the formation of other oxidants such as ozone (Eq. 7) .

$$^{\bullet}OH + {}^{\bullet}OH \rightarrow H_2O_2 \quad (4)$$

$HSO_4^- + {}^\bullet OH \rightarrow (SO_4^-)^\bullet + H_2O$ (5)

$(SO_4^-)^{\bullet\cdot} + {}^\bullet OH \rightarrow HSO_5^-$ (6)

$O_2 + 2\ {}^\bullet OH \rightarrow O_3 + H_2O$ (7)

Likewise, the recombination of free sulfate radicals is known to lead to the formation of peroxosulfate, as shown in Eq. (8). The recombination of $^\bullet OH$ can explain oxygen evolution (Eq. 9).

$(SO_4^-)^{\bullet\cdot} + (SO_4^-)^\bullet \rightarrow S_2O_8^{2-}$ (8)

$2\ {}^\bullet OH \rightarrow O_2 + 2\ H^+ + 2\ e^-$ (9)

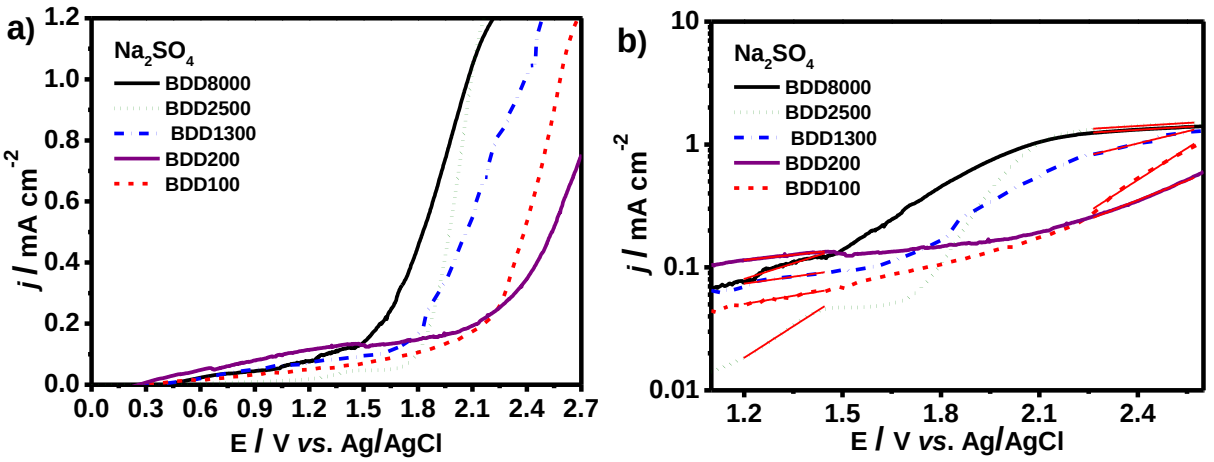

Figure 4. Linear sweep voltammetry curves (a) and Tafel plots (b) recorded in 3.0 g L^{-1} Na_2SO_4 at 5 mV s^{-1}.

Recently, Da Costa et al., 2019 studied the effect of the concentration of the supporting electrolyte (from 0.01 to 0.00001 mol L^{-1} H_2SO_4) and the role of oxidants in solution taking into consideration linear voltammetric measurements [33]. They also found two slopes for the linear sweep voltammetric curves obtained for the acidic solutions of 0.01 and 0.001 mol L^{-1} H_2SO_4. These two distinct linearity regions can be attributed to the sulfate ions in the solution transformed to persulfate and the hydroxyl radical formation on the surface of the BDD anode [31, 34]. These observations are in agreement with the observed behavior in Figure 4 for 0.021

mol L^{-1} (3.0 g L^{-1}) Na_2SO_4. In this case, for high sulfate ions content, occur mediated surface chemical steps that are responsible for the formation of persulfate ($S_2O_8^{2-}$), as described in Eq. (8). According to the literature, linearity is observed only at diluted solutions, indicating the prevalence of electrochemical reactions related to reactive oxygen species (e.g. hydroxyl radicals) [32, 33].

Table 4. Oxygen evolution overpotential of different BDDs studied in Na_2SO_4 media and Tafel slopes obtained from linear sweep voltammetry curves.

Anode	OER overpotential	$b_{sulfate}$ V dec^{-1}	R^2	b_{OER} V dec^{-1}	R^2
BDD8000	1.6 V	0.98	98.8	0.16	99.0
BDD2500	1.79 V	1.71	98.1	0.16	97.8
BDD1300	1.77 V	0.38	99.5	0.65	98.4
BDD200	1.72 V	0.28	92.0	1.06	99.6
BDD100	2.29 V	0.44	99.6	1.71	99.1

The significant differences in the onset of the OER for distinct BDD films should have a substantial effect on the formation of oxidants during bulk electrolysis. In order to evaluate this formation, an aqueous solution containing 3000 ppm Na_2SO_4 was electrolyzed at a fixed current density of 30 mA cm^{-2} (typical conditions in environmental applications) and with an electric charge passed of 6.4 A h dm^{-3} **(Figure 5).**

Higher doping level (2500 ppm and 8000 ppm) leads to lower oxidants formation as compared with the BDD100 and BDD200. The operation current densities correspond to the region in which the OER is the primary reaction. As pointed out before in this zone, hydroxyl radical formation is promoted with low boron doping. It means that both electrodes are expected to be more efficient than the highly doped films (which promoted the direct sulfate radical

formation). As hydroxyl radicals can indirectly promote the formation of sulfate radicals, almost no differences can be observed comparing the anodes. In fact, in the case of the BDD1300 (with a thicker layer), the formation of oxidants seems to be improved, and this may be explained by the higher surface area, which promotes the formation of stable oxidants from both sulfate and hydroxyl radicals. Although we previously point out that at these conditions, the concentrations of oxidants formed are very close to precisely affirming this effect.

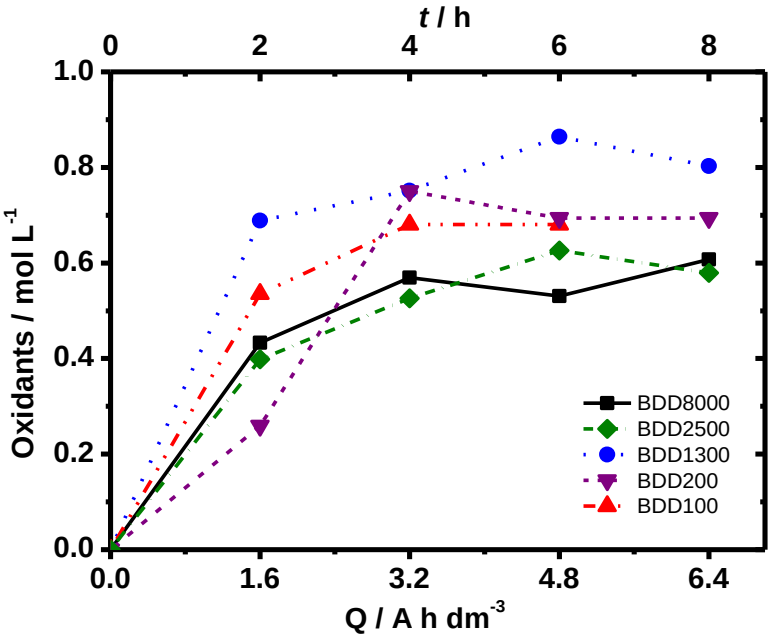

Figure 5. Variation of oxidants electro generated with the applied charge applied (Q) during the electrolysis at different BDD anodes. Na_2SO_4 = 3.0 g L^{-1}.

b. Reactive chlorine species formation

As it previously observed in Na_2SO_4 media, the OER overpotential decreases with the increasing boron doping level in NaCl **(Figure 6)**. A more positive OER overpotential of 2.42 V and 2.27 V was observed for BDD200 and BDD100, respectively, while 1.86 V, 1.90 V, and 2.12 V were found for BDD8000, BDD2500 and BDD1300. In the inset of Figure 6 are the Tafel plots. Two different processes also occur, which can be associated with the formation of chloride and hydroxyl radicals, respectively. As in the case of the Na_2SO_4 media, the shift of the plots corresponds to the overlapping of the OER with the chloride oxidation. Table 5

presents the fitting values of the two Tafel slopes. Mostafa *et al.*, 2018 compared electrolysis in 0.6 mol L^{-1} $NaClO_4$ or 0.6 mol L^{-1} NaCl. Data evidenced the competition between the electrogeneration of $^{\bullet}OH$ radicals (O_2 evolution) and the Cl_2 evolution during electrolysis in the presence of chlorides ions [35]. Likewise, here, similar behavior is observed for a more dilute chloride concentration (i.e., 0.064 mol L^{-1} or 3.7 g L^{-1} NaCl).

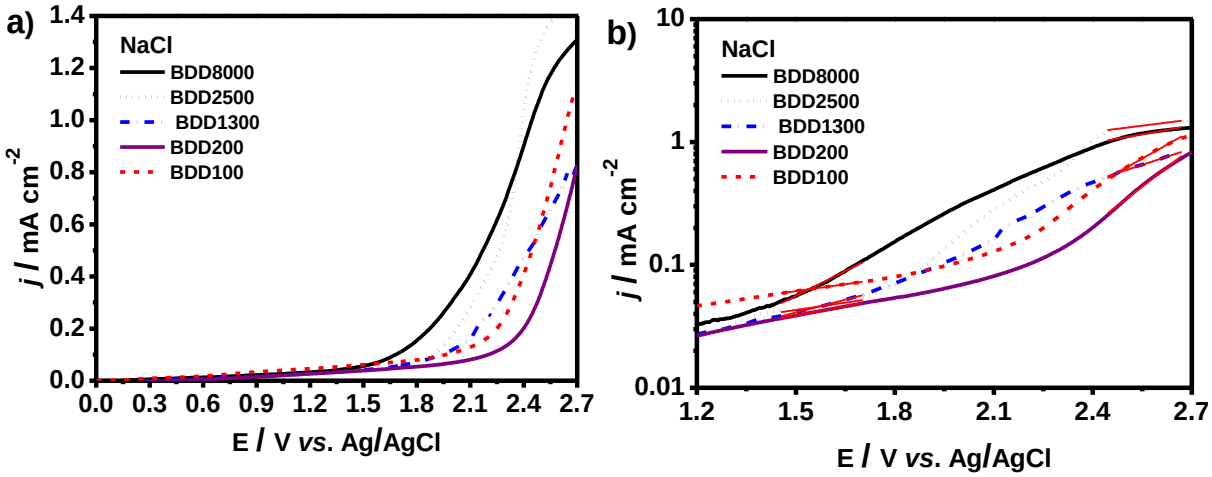

Figure 6. Linear sweep voltammetry curves (a) and Tafel plots (b) recorded in 3.7 g L^{-1} NaCl at 5 mV s^{-1}.

Table 5. Oxygen evolution potential of different BDDs studied in NaCl media and Tafel slopes obtained from linear sweep voltammetry curves.

Anode	OER overpotential	$b_{chlorine}$ V dec^{-1}	R^2	b_{OER} V dec^{-1}	R^2
BDD8000	1.86	1.10	99.5	0.47	96.4
BDD2500	1.9	0.39	98.7	0.39	92.4
BDD1300	2.12	0.65	99.7	0.90	99.4
BDD200	2.42	0.49	99.9	1.32	99.8
BDD100	2.27	0.39	98.9	1.54	99.6

During electrolysis of aqueous solutions containing chlorides, these anions are expected to be oxidized to chlorine (Eq. 10), and then, chlorine can disproportionate to yield hypochlorite (Eq. 11) .

$$2\ Cl^- \rightarrow Cl_2 + 2\ e^- \quad (10)$$

$$Cl_2 + OH^- \rightarrow ClO^- + Cl^- + H^+ \quad (11)$$

In the literature [17], it is demonstrated that direct oxidation of chlorine or hypochlorite to higher oxidation states is unfavored, as compared to the formation of chlorine. However, these processes can occur extensively by hydroxyl radicals mediated oxidation, as indicated in Eqs. (12)–(15). It is one of the main drawbacks of the electrolysis of water with diamond anodes because of the high hazardousness of both species [36, 37].

$$Cl^- + {}^{\bullet}OH \rightarrow ClO^- + H^+ + e^- \quad (12)$$

$$ClO^- + {}^{\bullet}OH \rightarrow ClO_2^- + H^+ + e^- \quad (13)$$

$$ClO_2^- + {}^{\bullet}OH \rightarrow ClO_3^- + H^+ + e^- \quad (14)$$

$$ClO_3^- + {}^{\bullet}OH \rightarrow ClO_4^- + H^+ + e^- \quad (15)$$

Similar experiments than the made for Figure 5 were repeated in a solution containing 3.7 g L^{-1} NaCl. The variation of chlorine compounds with the current charge applied (Q) during electrolysis at BDD8000 and BDD100 **(Figure 7)** is shown, as representative of the behavior for the higher and lower doping level ranges. The trend observed for the concentrations of chlorine species with time is in accordance with other studies in the literature: the chloride concentration decreases at the same time that oxidizing species are generated [38, 39]. **Table 6** shows the kinetics rate of chlorine species formation.

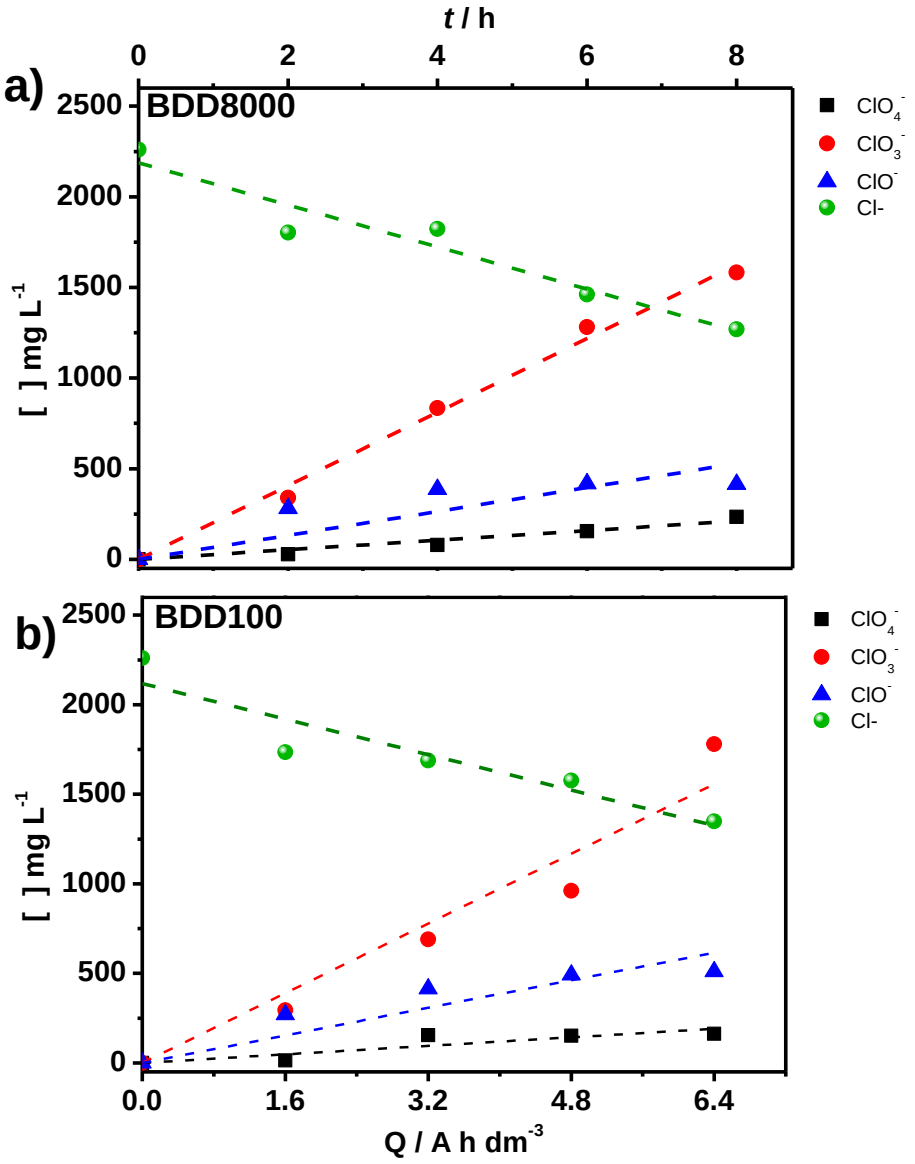

Figure 7. Variation of chlorine compounds with the applied charge applied (Q) during electrolysis at BDD8000 (a) and BDD100 (b). NaCl = 3.7 g L^{-1}.

According to the linear voltammetry curves (**Figure 6**), the oxidation of chlorides was expected to be less critical as the boron doping level decreases. Conversely, the formation of hydroxyl radicals was expected to be favored in this direction (as it was commented before regarding the formation of oxidative sulfate species). Thus, these opposite trends can help to explain that general behavior leads to insignificant differences due to the doping level. It occurs because the action of the hydroxyl radicals entirely masks this behavior, showing in all cases the vital

formation of chlorates and perchlorates. As in the case of sulfates, chlorides can be easily oxidized by hydroxyl radicals, yielding not only hypochlorite but also chlorates and perchlorates. Hence, within the conditions used, it is impracticable to discern between the chlorine oxidative species formed on the surface by direct transfer of electrons and those formed by mediated hydroxyl radical oxidation, although this latter should be primary, because of the observed extensive formation of perchlorates. In this context, the voltammetric study indicates that the action of the hydroxyl radicals can be essential in order to justify the presence of chlorates and perchlorates. If these hazardous species are to be prevented, it is necessary to use very soft conditions in which these hydroxyl radicals are not extensively formed. It is because there is a range in which the direct oxidation of chloride is favored before the formation of hydroxyl radicals. It is related to previous observations made by our group [40-42], in which it was found that formation of chlorates and perchlorate during disinfection of water can be avoided easily, only by working at very low current densities, just in a voltage region in which the hydroxyl radical formation is unfavored. Here, the results obtained to support this explanation and point out that to prevent perchlorates, it is not only needed to operate at very low current densities but also to use diamond coatings with very high boron doping levels.

Table 6. Reactive chlorine rate formation of species formed during electrolysis of NaCl solution.

Anode	ClO_4		ClO_3		ClO	
	mg Cl L^{-1} h	R^2	mg Cl L^{-1} h	R^2	mg Cl L^{-1} h	R^2
BDD8000	9.39	97.27	86.27	99.7	45.45	89.0
BDD2500	12.7	94.70	76.21	99.6	48.43	81.9
BDD1300	11.5 ± 6.4	90.11	85.54±5.6	99.9	64.55±1.5	91.8
BDD200	4.8 ± 0.42	97.5	93.20	99.5	61.02	91.8
BDD100	8.5	90.55	82.65	97.07	52.97	93.8

4. Conclusions

From this work, the following conclusions can be drawn:

- Boron doping affects the physical characteristics of the surface of BDD electrodes. The higher the boron doping, the higher is the hydrophilic behavior, and the lower is the crystallite size, which, in turn, can help to explain the higher conductivity of the electrodes.
- The physical characteristics of the BDD influence on their electrochemical responses. Higher boron doping levels promote electron transfer activity. The higher doping levels (8000–1300 ppm) exhibit semi-metallic conductivity due to the impurity bands of low energy that allow electron conduction, which is reflected in the lower charge transfer resistance. The lower doping levels (100 and 200 ppm) exhibit semi-conductive properties with low conductivity, as shown by the higher charge transfer resistance.
- Low boron doping favors the formation of hydroxyl radicals, while higher doping levels favor the direct oxidation of sulfate and chloride on the surface of the diamond electrodes. However, when operating at high overpotentials in bulk electrolysis, the formation of chlorine and sulfate oxidative species is favored at low boron doping levels, because of the very efficient mediated formation of these oxidants by reaction with hydroxyl radicals.
- The thickness of the BDD layer and Si-resistivity can influence the electron-transfer ability of BDD anodes, even more than the boron doping level. Thus, the higher thickness of the BDD1300 used in this study can help to explain the higher concentration of oxidants formed with this electrode.

Acknowledgments

Financial support from the Spanish Ministry of Economy, Industry and Competitiveness and European Union through project CTQ2017-91190-EXP (AEI/FEDER, UE) is gratefully acknowledged, as well as the Brazilian agencies CNPq (305438/2018-2, and 310282/2013-6), CAPES (99999.008454/2014-00 and 88887.142044/2017-00) and FAPITEC/SE.

References

[1] E. Brillas, C.A. Mart, Synthetic diamond films: preparation, electrochemistry, characterization, and applications, John Wiley & Sons2011.

[2] S.O. Ganiyu, E.V. dos Santos, E.C.T. de Araújo Costa, C.A. Martínez-Huitle, Electrochemical advanced oxidation processes (EAOPs) as alternative treatment techniques for carwash wastewater reclamation, Chemosphere 211 (2018) 998-1006.

[3] E. Brillas, C.A. Martínez-Huitle, Decontamination of wastewaters containing synthetic organic dyes by electrochemical methods. An updated review, Applied Catalysis B: Environmental 166 (2015) 603-643.

[4] M.F. García-Montoya, S. Gutiérrez-Granados, A. Alatorre-Ordaz, R. Galindo, R. Ornelas, J.M. Peralta-Hernandez, Application of electrochemical/BDD process for the treatment wastewater effluents containing pharmaceutical compounds, Journal of Industrial and Engineering Chemistry 31 (2015) 238-243.

[5] S.O. Ganiyu, C.A. Martínez-Huitle, Nature, Mechanisms and Reactivity of Electrogenerated Reactive Species at Thin-Film Boron-Doped Diamond (BDD) Electrodes During Electrochemical Wastewater Treatment, ChemElectroChem 6(9) (2019) 2379-2392.

[6] C.P. Sousa, F.W. Ribeiro, T.M. Oliveira, G.R. Salazar-Banda, P. de Lima-Neto, S. Morais, A.N. Correia, Electroanalysis of Pharmaceuticals on Boron-Doped Diamond Electrodes: A Review, ChemElectroChem 6(9) (2019) 2350-2378.

[7] K. Muzyka, J. Sun, T.H. Fereja, Y. Lan, W. Zhang, G. Xu, Boron-doped diamond: current progress and challenges in view of electroanalytical applications, Analytical methods 11(4) (2019) 397-414.

[8] K. Schwarzová-Pecková, J. Vosáhlová, J. Barek, I. Šloufová, E. Pavlova, V. Petrák, J. Zavázalová, Influence of boron content on the morphological, spectral, and electroanalytical

characteristics of anodically oxidized boron-doped diamond electrodes, Electrochimica Acta 243 (2017) 170-182.
[9] T.A. Ivandini, T. Watanabe, T. Matsui, Y. Ootani, S. Iizuka, R. Toyoshima, H. Kodama, H. Kondoh, Y. Tateyama, Y. Einaga, Influence of Surface Orientation on Electrochemical Properties of Boron-Doped Diamond, The Journal of Physical Chemistry C 123(9) (2019) 5336-5344.
[10] Z. Futera, T. Watanabe, Y. Einaga, Y. Tateyama, First principles calculation study on surfaces and water interfaces of boron-doped diamond, The Journal of Physical Chemistry C 118(38) (2014) 22040-22052.
[11] G.R. Salazar-Banda, L.S. Andrade, P.A. Nascente, P.S. Pizani, R.C. Rocha-Filho, L.A. Avaca, On the changing electrochemical behaviour of boron-doped diamond surfaces with time after cathodic pre-treatments, Electrochimica Acta 51(22) (2006) 4612-4619.
[12] J. Matsushima, W. Silva, A. Azevedo, M. Baldan, N. Ferreira, The influence of boron content on electroanalytical detection of nitrate using BDD electrodes, Applied Surface Science 256(3) (2009) 757-762.
[13] J. Radjenovic, D.L. Sedlak, Challenges and opportunities for electrochemical processes as next-generation technologies for the treatment of contaminated water, Environmental Science & Technology 49(19) (2015) 11292-11302.
[14] M. Cheng, G. Zeng, D. Huang, C. Lai, P. Xu, C. Zhang, Y. Liu, Hydroxyl radicals based advanced oxidation processes (AOPs) for remediation of soils contaminated with organic compounds: a review, Chemical Engineering Journal 284 (2016) 582-598.
[15] C.A. Martinez-Huitle, M.A. Rodrigo, I. Sires, O. Scialdone, Single and coupled electrochemical processes and reactors for the abatement of organic water pollutants: a critical review, Chemical reviews 115(24) (2015) 13362-13407.
[16] C. do Nascimento Brito, D.M. de Araújo, C.A. Martínez-Huitle, M.A. Rodrigo, Understanding active chlorine species production using boron doped diamond films with lower and higher sp3/sp2 ratio, Electrochemistry Communications 55 (2015) 34-38.
[17] A. Sánchez-Carretero, C. Sáez, P. Cañizares, M. Rodrigo, Electrochemical production of perchlorates using conductive diamond electrolyses, Chemical Engineering Journal 166(2) (2011) 710-714.
[18] E. Morillo, J. Villaverde, Advanced technologies for the remediation of pesticide-contaminated soils, Science of the Total Environment 586 (2017) 576-597.
[19] A. Kapałka, G. Fóti, C. Comninellis, Investigations of electrochemical oxygen transfer reaction on boron-doped diamond electrodes, Electrochimica Acta 53(4) (2007) 1954-1961.

[20] S. Ferro, A. De Battisti, I. Duo, C. Comninellis, W. Haenni, A. Perret, Chlorine evolution at highly boron-doped diamond electrodes, Journal of the Electrochemical Society 147(7) (2000) 2614-2619.
[21] M. Murata, T.A. Ivandini, M. Shibata, S. Nomura, A. Fujishima, Y. Einaga, Electrochemical detection of free chlorine at highly boron-doped diamond electrodes, Journal of Electroanalytical Chemistry 612(1) (2008) 29-36.
[22] M. Mertens, M. Mohr, K. Bruehne, H.-J. Fecht, M. Łojkowski, W. Święszkowski, W. Łojkowski, Patterned hydrophobic and hydrophilic surfaces of ultra-smooth nanocrystalline diamond layers, Applied Surface Science 390 (2016) 526-530.
[23] M.H. Santana, L.A.d. Faria, Oxygen and chlorine evolution on RuO {sub 2}+ TiO {sub 2}+ CeO {sub 2}+ Nb {sub 2} O {sub 5} mixed oxide electrodes, Electrochimica Acta 51 (2006) 3578–3585.
[24] A. Azevedo, M. Baldan, N. Ferreira, Doping level influence on chemical surface of diamond electrodes, Journal of Physics and Chemistry of Solids 74(4) (2013) 599-604.
[25] Z. Chen, Y. Jin, W. Yang, B. Xu, Y. Chen, X. Yin, Y. Liu, Fabrication and characterization of polypyrrole coatings by embedding antimony modified SnO2 nanoparticles, Journal of Industrial and Engineering Chemistry 75 (2019) 178-186.
[26] P. Cañizares, C. Sáez, A. Sánchez-Carretero, M. Rodrigo, Influence of the characteristics of p-Si BDD anodes on the efficiency of peroxodiphosphate electrosynthesis process, Electrochemistry Communications 10(4) (2008) 602-606.
[27] S. Ferro, A. De Battisti, Electron transfer reactions at conductive diamond electrodes, Electrochimica Acta 47(10) (2002) 1641-1649.
[28] J.A. Garrido, S. Nowy, A. Haertl, M. Stutzmann, The diamond/aqueous electrolyte interface: an impedance investigation, Langmuir 24(8) (2008) 3897-3904.
[29] E. Mahé, D. Devilliers, C. Comninellis, Electrochemical reactivity at graphitic micro-domains on polycrystalline boron doped diamond thin-films electrodes, Electrochimica acta 50(11) (2005) 2263-2277.
[30] E. Guinea, F. Centellas, E. Brillas, P. Cañizares, C. Sáez, M.A. Rodrigo, Electrocatalytic properties of diamond in the oxidation of a persistant pollutant, Applied Catalysis B: Environmental 89(3-4) (2009) 645-650.
[31] K. Serrano, P. Michaud, C. Comninellis, A. Savall, Electrochemical preparation of peroxodisulfuric acid using boron doped diamond thin film electrodes, Electrochimica Acta 48(4) (2002) 431-436.

[32] A. Kapałka, G. Fóti, C. Comninellis, Determination of the Tafel slope for oxygen evolution on boron-doped diamond electrodes, Electrochemistry Communications 10(4) (2008) 607-610.
[33] T.F. da Costa, J.E. Santos, D.R. da Silva, C.A. Martinez-Huitle, BDD-Electrolysis of Oxalic Acid in Diluted Acidic Solutions, J. Braz. Chem. Soc 30(7) (2019) 1541-1547.
[34] C. Zhang, Z. He, J. Wu, D. Fu, The peculiar roles of sulfate electrolytes in BDD anode cells, Journal of The Electrochemical Society 162(8) (2015) E85-E89.
[35] E. Mostafa, P. Reinsberg, S. Garcia-Segura, H. Baltruschat, Chlorine species evolution during electrochlorination on boron-doped diamond anodes: In-situ electrogeneration of Cl_2, Cl_2O and ClO_2, Electrochimica Acta 281 (2018) 831-840.
[36] M.H. Bergmann, J. Rollin, T. Iourtchouk, The occurrence of perchlorate during drinking water electrolysis using BDD anodes, Electrochimica Acta 54(7) (2009) 2102-2107.
[37] O. Azizi, D. Hubler, G. Schrader, J. Farrell, B.P. Chaplin, Mechanism of perchlorate formation on boron-doped diamond film anodes, Environmental science & technology 45(24) (2011) 10582-10590.
[38] A. Polcaro, A. Vacca, M. Mascia, F. Ferrara, Product and by-product formation in electrolysis of dilute chloride solutions, Journal of applied electrochemistry 38(7) (2008) 979-984.
[39] A. Polcaro, A. Vacca, M. Mascia, S. Palmas, J.R. Ruiz, Electrochemical treatment of waters with BDD anodes: kinetics of the reactions involving chlorides, Journal of Applied Electrochemistry 39(11) (2009) 2083.
[40] A. Cano, P. Cañizares, C. Barrera, C. Sáez, M. Rodrigo, Use of low current densities in electrolyses with conductive-diamond electrochemical—oxidation to disinfect treated wastewaters for reuse, Electrochemistry Communications 13(11) (2011) 1268-1270.
[41] A. Cano, P. Cañizares, C. Barrera-Díaz, C. Sáez, M.A. Rodrigo, Use of conductive-diamond electrochemical-oxidation for the disinfection of several actual treated wastewaters, Chemical engineering journal 211 (2012) 463-469.
[42] S. Cotillas, J. Llanos, M.A. Rodrigo, P. Cañizares, Use of carbon felt cathodes for the electrochemical reclamation of urban treated wastewaters, Applied Catalysis B: Environmental 162 (2015) 252-259.